Solar Energy Materials and Solar Cells 172 (2017) 368–375

Contents lists available at ScienceDirect

Solar Energy Materials and Solar Cells

journal homepage: www.elsevier.com/locate/solmat

Selection of anti-solvent and optimization of dropping volume for the preparation of large area sub-module perovskite solar cells

Kun-Mu Lee[a,b,c,*], Chuan-Jung Lin[d], Bo-Yi Liou[e], Sheng-Min Yu[d,f], Chien-Chung Hsu[d], Vembu Suryanarayanan[g], Ming-Chung Wu[a,b,c,*]

[a] Department of Chemical and Materials Engineering, Chang Gung University, Taoyuan 33302, Taiwan
[b] Division of Neonatology, Department of Pediatrics, Chang Gung Memorial Hospital, Taoyuan 33305, Taiwan
[c] Center for Reliability Sciences and Technologies, Chang Gung University, Taoyuan 33302, Taiwan
[d] Department of Engineering and Science, National Tsing Hua University, Hsinchu 30013, Taiwan
[e] Department of Chemical and Materials Engineering, National Central University, Taoyuan 320, Taiwan
[f] Material and Chemical Research Laboratory, Industrial Technology Research Institute (ITRI), Hsinchu 31040, Taiwan
[g] Electro Organic Division, Central Electrochemical Research Institute, Karaikudi 630006, Tamil Nadu, India

ARTICLE INFO

Keywords:
Anti-solvent
Perovskite
Solar cells
Large area
Sub-module

ABSTRACT

Anti-solvents play a critical role on the preparation of perovskite active layers for photovoltaic applications. This work explores the treatment of various anti-solvents for adjusting the crystallinity and morphology of perovskite active layer. It is found that the anti-solvent with a low dielectric constant and dipole moment is the most suitable one for the preparation of perovskite layer. It is also noted that the optimal volume ratio of the perovskite precursor to toluene as an anti-solvent is 1:3. Using toluene as the anti-solvent, the perovskite solar cells (p-i-n type) are fabricated with a single cell and a sub-module within an active area of 0.10 cm^2 and 11.25 cm^2, respectively. Such display exhibits impressive power conversion efficiencies (PCE) of 13.12% and 11.60% with negligible *J-V* hysteresis, respectively, under the illumination of 100 mW/cm^2 (AM1.5G).

1. Introduction

Recently, the organic-inorganic hybrid perovskite ($CH_3NH_3PbI_3$; $MAPbI_3$) photovoltaic devices have attracted a lot of attention, as its power conversion efficiency (PCE) has leapt from 3.8% in 2009 [1] to the current world record of 22.1% [2]. This is attributed to its outstanding optoelectronic characteristics, including high absorption coefficient [3], low exciton binding energy of ~0.03 eV [4], long carrier diffusion length [5], and tunable energy bandgap [6]. Because of these properties, the perovskite materials are considered as suitable light absorbers in the field of solar cells as well as light-emitting devices [7]. Typically, organic-inorganic perovskite has an ABX_3 crystal structure, where the organic cations usually locate at the A site, the smaller divalent metal ions insert into the B site, and X is usually a halide ion. In hybrid organic-inorganic perovskite, methylammonium ($CH_3NH_3^+$; MA^+) or formamidinium ($HC(NH_2)_2^+$; FA^+) typically serves as the organic cation. Lead (Pb^{2+}) or tin (Sn^{2+}) acts as small divalent metal ion with the halide ions such as I^-, Cl^-, and Br^- [6]. Various perovskite film preparation methods are well-developed, such as one-step solution process [8], sequential deposition [9], dual-source vapor deposition [10], and a vapor-assisted solution process [11]. Perovskite materials deposited onto mesoporous metal oxides (TiO_2) displaying a high PCE (22.1%) have been widely studied, describing how the metal oxide acts as a scaffold, improving perovskite coverage [8]. Conversely, inverted planar perovskite solar cells have also been extensively researched. The inverted perovskite solar cells have some advantages such as simple as well as low temperature device fabrication, high stability and small hysteresis [12–14]. However, perovskite material directly coated onto a hole transport material (HTM)-modified substrate is hardly to form a homogenous perovskite layer. This results from the difference between the nucleation and the grain growth rates [15,16]. The PCEs of inverted perovskite photovoltaic devices are usually lower than those of normal-structured perovskite photovoltaic devices, especially on the reporting of independently certified results [17,18]. Typically, the heterogeneous nucleation appears in a one-step solution process due to the early crystallization of perovskite material, generating differently sized perovskite crystals on the substrate. Thus, suppressing perovskite crystal grain growth rate becomes an important issue. Replacing dimethylformamide (DMF) by dimethyl sulfoxide (DMSO) leads to a PCE of 13.5% in order to retard the perovskite crystal grain growth rate [19]. Similarly, using a hydroiodic acid (HI) pre-treatment to form new $HPbI_3$ compounds results in a PCE of 17.5% [20]. However, hysteresis

* Corresponding authors at: Department of Chemical and Materials Engineering, Chang Gung University, Taoyuan 33302, Taiwan.
E-mail addresses: kmlee@mail.cgu.edu.tw (K.-M. Lee), mingchungwu@mail.cgu.edu.tw (M.-C. Wu).

http://dx.doi.org/10.1016/j.solmat.2017.08.010
Received 9 May 2017; Received in revised form 21 July 2017; Accepted 8 August 2017
Available online 19 August 2017

phenomena exist in perovskite solar cells due to residual HI, DMSO, or PbI_2 compounds. An efficient anti-solvent, that aided the preparation of homogenous large-grained perovskite film, was proposed by Seok *et al.* [21]. In this approach, all the elements were doped into a perovskite film after the removal of the residual DMSO which formed a new complex as an intermediate phase of $MA_2Pb_3I_8(DMSO)_2$ instead of DMSO-PbI_2-CH_3NH_3I with 1:1:1 stoichiometry [22]. Finally, after post-annealing at 100 °C for 10 min, the complex was fully converted into a highly crystalline perovskite layer with uniform perovskite grain distribution. As previously reported, the anti-solvent baths and micro-flow anti-solvent methods for the fabrication of ultra-smooth perovskite films with the full coverage and the smooth surface roughness have been proposed by Bin Xia et al. and Yuanyuan Zhou et al.[23,24]. Large number of chemicals can be used as anti-solvents. However, the choice and other conditions of anti-solvents for preparing perovskite film are not very clear. Therefore, selection of the anti-solvent and its dropping volume become a significant factor when fabricating high-performance perovskite photovoltaic devices. In the previous works, the most suitable anti-solvent used is toluene (TL) for the preparation perovskite layer [21]. However, most of the works have not addressed the impact of the anti-solvent species and their amount used during preparation of perovskite layer process. In this work, we have developed a systematic study for determining the suitability of several of anti-solvents on the perovskite active layer including toluene (TL), chlorobenzene (CB), chloroform (CF), dichlorobenzene (DCB), isopropyl alcohol (IPA), and some common organic solvents. It is found that the most suitable anti-solvent for the preparation of perovskite solar cell is toluene since it drives the perovskite precursor into the metastable zone instead of the supersaturation zone. This is in good agreement with the report [21]. Furthermore, it is observed that the dropping volume ratio of perovskite precursor to anti-solvent (TL) is 1:3 (v: v), which is the optimal condition for the preparation of perovskite solar cells (the substrate area is 2.5 cm^2). The TL dropping volume influences the film morphology and crystallization obviously, where the optimal dropping volume can generate the largest perovskite grain size (~500 nm) and flat surface. It benefits the subsequent layers such as PCBM or sliver metal contact. If the TL dropping volume is excessive or less, a huge of tiny perovskite crystals or discontinuous perovskite layers are formed after post-annealing. In the final section, TL was used as an anti-solvent and the volume ratio was kept to prepare a sub-module (larger-area, the substrate area is 25 cm^2) perovskite solar cell. This perovskite photovoltaic device shows power conversion efficiency as high as 11.60% with negligible J-V hysteresis.

2. Experimental section

2.1. Material preparation

CH_3NH_3I (MAI) was synthesized by reacting 27.86 ml CH_3NH_2 (40% in methanol, Aldrich) and 30 ml HI (57 wt% in water, Aldrich) in a 250 ml round-bottom flask at 0 °C for 4 h with stirring. The precipitate was recovered by evaporation at 55 °C for 1 h. The MAI was then dissolved in ethanol, recrystallized from diethyl ether, and dried at 60 °C in a vacuum oven for 24 h. The perovskite precursor solution was prepared by mixing PbI_2 and CH_3NH_3I at molar ratio of 1:1 in a co-solvent system of dimethylsulfoxide (DMSO): γ-butyrolactone (GBL) (volume ratio of 5:5) with a total concentration of 20 wt%.

2.2. Solar cell fabrication

The pre-patterned ITO-coated substrate, with a sheet resistance of 7 Ω/square, was cleaned with a neutral wash solution (Extran® MA 02, Merck Inc.), acetone, and isopropyl alcohol. The substrate was dried at 80 °C for 24 h followed by treatment with UV-ozone for 10 min, Then, it was spin-coated with a PEDOT: PSS (Heraeus Clevios™ P VP AI 4083) solution at 5000 rpm for 50 s, and baked at 120 °C for 10 min in an ambient conditions. After that, the sample was immediately transferred to a nitrogen-filled glove box for perovskite layer and PCBM layer preparation. The perovskite layer preparation involved a consecutive two-step spin-coating process, where it was conducted at 1000 and 5000 rpm for 10 s and 20 s, respectively, and the volume of the perovskite precursor was kept in 25 µl [21]. During the second spin-coating step, the perovskite layer was treated with different anti-solvents in the volume of 75 µl, and those solvents are summarized in Table S1. Following this, the perovskite layer was annealed at 100 °C for 10 min. A solution of PCBM in chlorobenzene (4 mg/ml) was spin-coated onto the perovskite layer. Finally, a 100 nm-thick silver (Ag) layer, using thermal evaporation, was deposited as the metal electrode. The active area (0.10 cm^2) of the solar cell was defined by using a shadow mask during Ag evaporation.

2.3. Characterization

UV–vis absorption spectra of all samples were measured with a U-4100, Hitachi UV–vis spectrophotometer. GIXRD data were collected in the 2-theta range of 10–50° with a Brucker powder diffractometer (D8 Discover) equipped with a 2D detector using CuKα1 radiation. The scanning electron micrographs (SEM) were obtained using a Hitachi S-800 microscope at 10.0 kV. The solar simulator used in this study was a 3 A (AAA) Wacom solar simulator (KXL-500F, Wacom, Japan). An NREL-certified silicon solar cell (Oriel, 91150 V) with a KG-5 bandpass filter was used to measure the optical intensity of simulated sunlight, and we fixed the optical intensity at 100 mW/cm^2 (AM 1.5 G). The J-V characteristics of devices were estimated by a computer-controlled digital source meter (Keithley 2400) under 100 mW/cm^2 (AM 1.5 G).

3. Results and discussion

3.1. Influence of the anti-solvent species

In order to facilitate comparison, the volumes of the perovskite precursor and the anti-solvent are set at 25µl and 75µl, respectively. Fig. 1**(a)** shows a diagram for the preparation process of uniform, large-grained and dense perovskite film. The process consists of five steps. First, CH_3NH_3I and PbI_2 are dissolved into a GBL: DMSO (v: v = 5:5) mixture as the perovskite precursor; Second, 25µl of the perovskite precursor in volume is dropped onto a PEDOT: PSS coated-ITO substrate; Third, the first step spin-coating process is run at 1000 rpm for 10 s; Fourth, the second step spin-coating process is run at 5000 rpm for 20 s. At the 17th second of the second step spin-coating process, the anti-solvent with 75µl in volume is dropped directly onto the substrate. In this step, the excess constituents, such as MAI, PbI_2, GBL, or DMSO, are removed and formed a new complex as an intermediate phase [21]. Finally, the anti-solvent-treated sample is placed on a hot plate for post-annealing. Fig. 1**(b)** shows photographs taken after the anti-solvent treatment and post-annealing process. From these photographs, it can be seen that some solvents, such as acetonitrile, γ-butyrolactone, methanol, tetrahydrofuran, N, N-dimethylformamide, and dimethyl sulfoxide, are not suitable as anti-solvents for the preparation of perovskite layer since they attack and dissolve the perovskite precursor. We believe that the anti-solvent solution plays a critical role during perovskite layer formation. These anti-solvent solutions can strongly affect the surface morphology and coverage as well as the crystallization kinetics [25]. Thus, the choice of an anti-solvent solution is important when preparing perovskite solar cells. As previously reported, the anti-solvent can significantly reduce the solubility of the solute in solution, but does not completely inhibit it, where it also accelerates homogenous nucleation due to supersaturation [21,26,27]. It is evident that the hybrid perovskite is hydrophilic and insoluble in nonpolar solvents. Here, only five anti-solvents such as toluene, chloroform, chlorobenzene, dichlorobenzene, and isopropyl alcohol are considered as suitable washing solvents for perovskite layer fabrication and studies have been

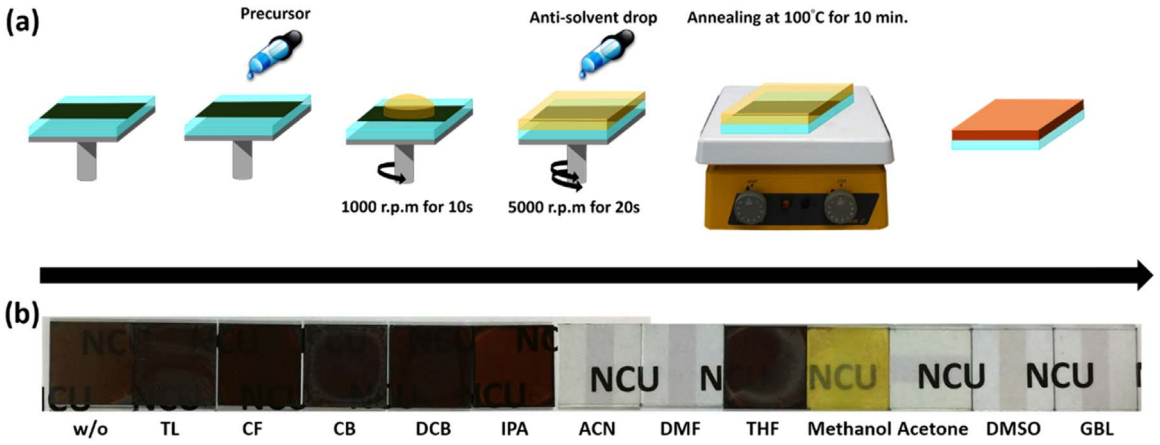

Fig. 1. (a) The diagram representing the preparation of perovskite layers. (b) the photographs of perovskite films were taken after the anti-solvent treatment and post-annealing.

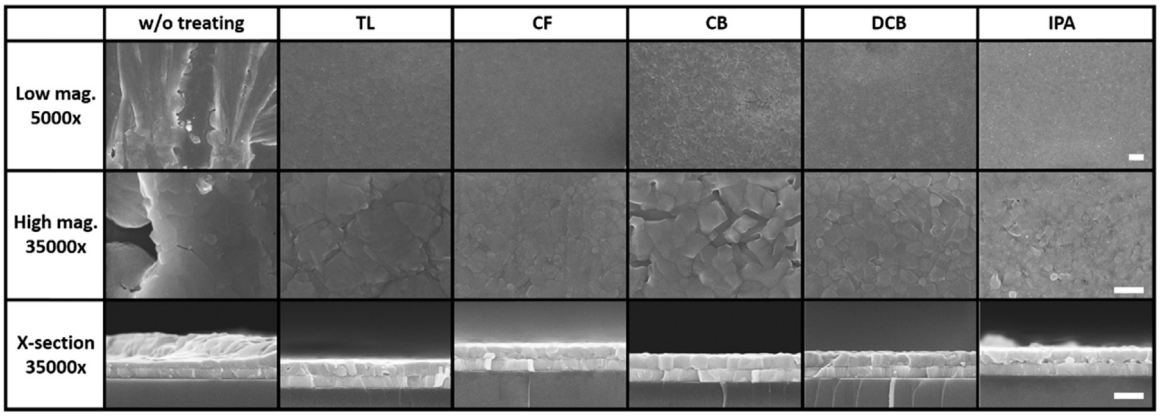

Fig. 2. The first row shows the top-view scanning electron microscopy (SEM) images without the anti-solvent treatment (w/o treatment), TL, CF, CB, DCB, and IPA at a low magnification of 5000×. The second row displays high-magnification SEM top-view images (35,000×). The cross-section (X-section) SEM images of w/o treatment, TL, CF, CB, DCB, and IPA, respectively, are shown in the third row. The scale bar equals 500 nm.

performed on the perovskite film formation in detail.

The microstructures of the anti-solvent treated and untreated (w/o) perovskite layers are shown in Fig. 2. The untreated perovskite layer shows dendritic structures with pin-holes indicating poor surface coverage, as shown in the first column of Fig. 2. This may be attributed to the uncoordinated nucleation and grain growth rate of perovskite. The surface coverage changes significantly when the anti-solvents are introduced [26]. After TL treatment, the PEDOT: PSS coated-ITO substrate has entirely covered with large perovskite grains, as shown in the second column of Fig. 2. When CF is introduced into the process, the perovskite grains develop a uniform distribution, becoming flatter than those from the untreated solution. Since the CF has small molar volume, it mixes with the DMSO/GBL solution more quickly than TL, and drives the perovskite precursor solution into supersaturation zone [28]. But, the size of perovskite grain is too small, and it indicates that a lot of grain boundaries exist in the perovskite layer. This may result in resistance during charge transportation in the perovskite layer [15,29]. Moreover, many deep pits occur on the perovskite layer surface after CB treatment, implying that the perovskite nucleation and grain growth rate may be slightly different. We believe that the deep pits will affect the coverage of subsequent layers such as PCBM or silver metal contact. The perovskite layer treated with DCB shows good coverage and uniform grain size. In addition, a huge number of tiny perovskite grains covered on the PEDOT: PSS coated-ITO substrate result in pinholes appearing on the surface during the treatment with IPA. It is evident that different surface morphologies and crystalline properties can be obtained by the treatment with different anti-solvents.

The anti-solvent crystallization technique is widely used in the pharmaceutical industry to synthesize drugs by crystallizing those from an original solvent. With the addition of an anti-solvent, the solute becomes relatively insoluble. The anti-solvent is soluble in the original solvent, leading the original solution to change from the under-supersaturation zone into the metastable zone or the supersaturation zone. Thus, the nucleation rate and grain growth of the drug can be controlled by the type or volume of the anti-solvent. Similarly, when the anti-solvent is introduced into the perovskite layer during manufacturing process, the solubility of the perovskite precursor decreases, since most of the solutions in the perovskite precursor are removed or diluted, depending on the dielectric constant and dipole moment of the anti-solvent [21,30,31]. This drives the perovskite precursor solution from the under-supersaturation zone into the metastable zone (TL) or the supersaturation zone (CF, CB, DCB, or IPA). The schematic diagram taken and modified from the literature reference with prior permission from the authors depicting the relative position of the various anti-solvents (not the absolute position) with different areas of distribution is shown in Fig. 3 [36]. When the perovskite precursor solution is treated with TL, the perovskite layer obtained is transparent, indicating the existence of a non-stoichiometric intermediate phase ($MA_2Pb_3I_8(DMSO)_2$) instead of DMSO-PbI_2-CH_3NH_3I with 1:1:1 stoichiometry (Fig. 3, **inset**) [22]. Thus, the consistent rate of nucleation and grain growth yields large uniform grains when the perovskite precursor solution is treated with TL. In contrast, when the perovskite precursor solution is treated with CF, CB, or DCB, the color of the perovskite layer is brown or light brown, which indicates that the perovskite crystals have directly been separated out during the anti-solvent treatment. This generates highly nucleation density, leading to

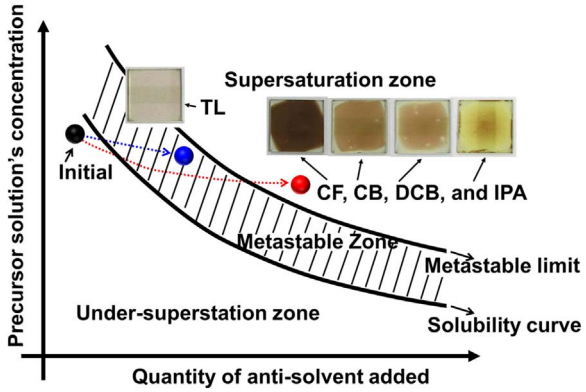

Fig. 3. The schematic diagram of the perovskite precursor concentration with respect to various anti-solvents. The inserts photos are taken from the perovskite precursor treatment with TL, CF, CB, DCB, and IPA before post-annealing [36].

a nucleation rate that is faster than the rate of grain growth. Thus, the grain size of the perovskite obtained is smaller than those obtained by the treatment with TL. A yellow-brown color was observed when the perovskite precursor solution was treated with IPA. This indicates that the PbI_2 and perovskite crystals separate out simultaneously since the most of MAI is dissolved and removed by IPA, resulting in inconsistent rates of nucleation and grain growth [32].

UV/vis spectroscopy was used to evaluate the perovskite layers before post-annealing, and the absorption spectra in different anti-solvents are shown in Fig. 4. The perovskite precursor solution treated with TL exhibits very low absorption in the range of 400–900 nm, and has been verified as a non-stoichiometric intermediate-phase absorption spectrum [22]. This confirms that the perovskite precursor solution is driven into the metastable zone upon by the addition of TL. In contrast, when the perovskite precursor solution is treated with CF, CB, or DCB, a typical perovskite absorption spectrum is obtained. This demonstrates again that the perovskite crystals directly separate out during the anti-solvent treatment. The absorption spectrum for the sample treated with IPA is similar to those of PbI_2 and a perovskite. This indicates that, not only that most of the MAI has been dissolved and is removed by the IPA, but also that some of the perovskite crystals are generated during the anti-solvent treatment [25].

Based on the above results, it can be concluded that: (a) the anti-solvent with a low dielectric constant and low dipole moment (TL) can drive the perovskite precursor solution from the under-supersaturation zone into the metastable zone, and exists as stable one in the intermediate-phase; (b) anti-solvents with dielectric constants and dipole moments that are slightly higher than TL (CF, CB, DCB), can drive the

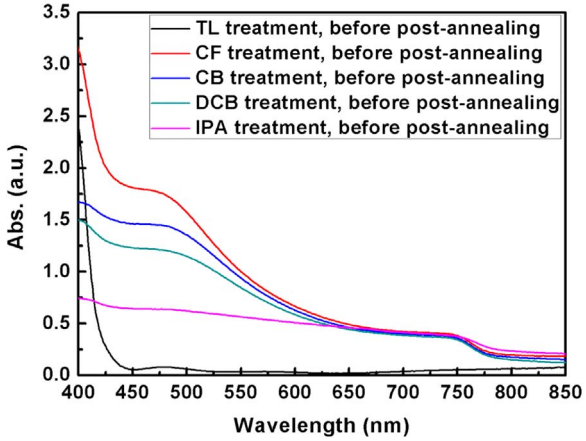

Fig. 4. The absorption spectra acquired from the perovskite precursor treated with various anti-solvents before post-annealing.

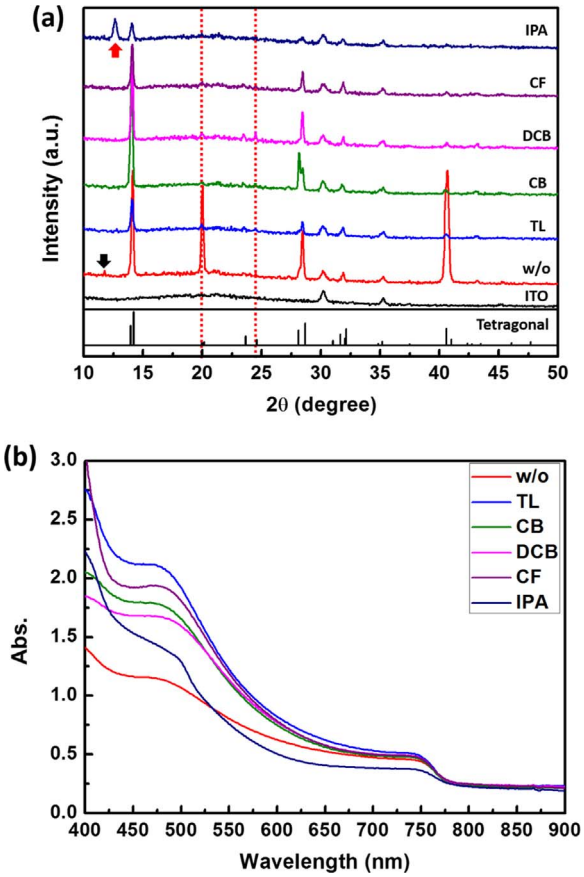

Fig. 5. (a) X-ray diffraction patterns and (b) UV–vis absorption spectra of the perovskite precursor treated with various anti-solvents after post-annealing.

perovskite precursor solution into the supersaturation zone. In this case, the perovskite crystals bypass the intermediate-phase and directly separate out; (c) when the anti-solvent has a higher dielectric constant with a dipole moment slightly higher than TL and PbI_2, some of the perovskite crystals separate out, since the most of the solution and MAI are dissolved and removed, leading to changes in the stoichiometry.

The XRD patterns of the samples before and after treatment with various anti-solvents are shown in Fig. 5**(a)**. Before the anti-solvent treatment, the intensity of perovskite layer is higher than the others indicating relatively high crystallinity. However, a small peak appears in the diffraction pattern corresponding to the intermediate-phase (black arrow) [20,22,33]. Moreover, its surface coverage is extremely poor and so it is not considered as a good candidate for perovskite solar cell application. After anti-solvent treatment, the X-ray diffraction peaks located at 2θ of 14.2°, 19.5°, 24.0°, 27.9°, 31.4°, 40.2°, 42.7°, and 49.9° indicate the formation tetragonal phase perovskite layer. It is worth to note that two extra higher orders of diffraction peaks appear at 19.5° (210) and 24.0° (202) (dashed red line). By comparing the simulated perovskite XRD diffraction pattern, these two extra higher orders of diffraction peaks indicate that the perovskite film treatment with the anti-solvent solutions is highly crystalline in nature [34]. The PbI_2 peak appears at 2θ of 12.5° (red arrow) corresponding to (100) when the perovskite precursor treats with IPA. This may be attributed to the stoichiometric change as a result of replacement of MAI by IPA solution. Fig. 5**(b)** shows the UV–vis absorption spectra of perovskite layers obtained by treatment with various anti-solvents and after post-annealing. The absorption curves cover a wide range of wavelengths from the visible to the near-infrared. For the perovskite layer treated with anti-solvents, the absorption edges are very sharp, consistent with their crystallinity. The untreated perovskite layer shows low absorption intensity because of the poor surface coverage and the embedded PbI_2

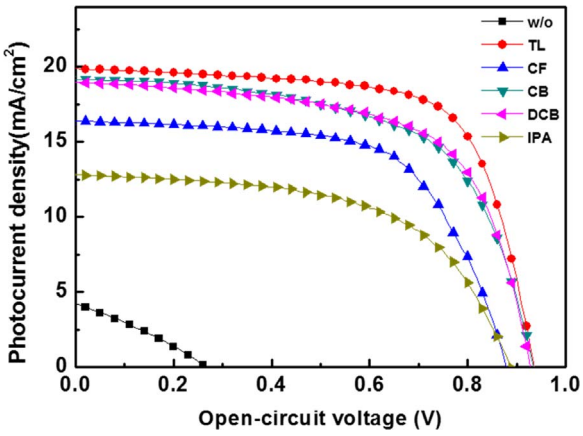

Fig. 6. The J–V characteristics obtained for the perovskite solar cells fabricated with different anti-solvent treatments (active area: 0.1 cm^2).

phase. Despite the fact that the absorption spectra of TL, CB, DCB, and CF are almost the same, the wavelength range of 400–600 nm is slightly different. This may be attributed to the pits in the perovskite layer or the surface roughness, even though the crystal structure (tetragonal) and thickness (~240 nm) are almost identical. Furthermore, the PbI_2 phase in the perovskite layer treated with IPA leads to a lower relative absorption spectrum.

The photovoltaic characteristics of typical small-area perovskite solar cells (0.10 cm^2) treated with different anti-solvents were primarily evaluated under AM 1.5 G irradiation at 100 mW/cm^2 and are shown in Fig. 6. Use of TL as the anti-solvent results in the highest PCE of 13.12% than those treated with CF, CB, or DCB.

The highest PCE is attributed to the anti-solvent of TL driving the perovskite precursor into the metastable zone, which results in the consistent rate of nucleation and grain growth at annealing process. Thus, a uniform and large grain perovskite layer can be obtained by TL anti-solvent treatment. Furthermore, the perovskite solar cells treatment with TL shows the highest fill factor of about 70%, contributing few amounts of grain boundaries. It has also been demonstrated by SEM top-view image. In contrast to the anti-solvent of TL, the lower PCE for the device used with CF, CB, and DCB may be attributed to the number of grain boundaries existing in the perovskite layer. This results in charge recombination as the perovskite crystal is directly formed by bypassing the intermediated-phase during the perovskite precursor treatment with CF, CB, or DCB. This indicates that the perovskite layer has higher nucleation density than that of TL treatment so that this generates high grain boundaries in the perovskite layer during grain growth.

In contrast to the untreated and IPA-treated samples, the PCE is significantly lower than the others. This may be attributed to the huge amount of PbI_2 and pin-holes embedded in the perovskite layer, leading to the formation of a carrier recombination center. Moreover, the energy levels of the anti-solvent treated perovskite films will be changed, which affect the carriers transport properties. The photovoltaic parameters of perovskite device fabricated with various anti-solvent treatments are summarized in Table 1. Based on above and photovoltaic characteristic results, we believe that the anti-solvent with a low dielectric constant and low dipole moment is the most suitable one for perovskite layer fabrication. It drives the perovskite precursor into the metastable zone instead of the supersaturation zone, leading to the nucleation rate and grain growth rate accordingly.

3.2. The effect of TL dropping volume

From the above evaluation, it is concluded that TL is a good anti-solvent candidate for the fabrication of perovskite photovoltaic device. In this section, it is focused on the TL dropping volume during the perovskite layer preparation process. In order to investigate the TL dropping volume effect, the perovskite precursor solution is kept at 25 μl, and other parameters are kept at the same. The TL dropping volumes used in this section are 25, 50, 75, and 100 μl. Fig. S1 shows the photographs of the perovskite precursor treated by TL with various dropping volumes before and after post-annealing. The perovskite precursors before post-annealing are transparent, indicating the metastable zone nature of the perovskite films [21]. However, when the as-treated samples are subjected to post-annealing at 100 °C for 10 min, the perovskite precursor treated with 25 μl of TL shows a white ring on the perovskite layer surface. This could be caused by residual MAI or pinholes and surface roughness [35]. When MAI is present on the perovskite layer surface, it becomes a carrier recombination center. Moreover, when the dropping volume is increased to 50, 75 and 100 μl, the white ring disappears and a dark-brown perovskite layer with a mirror-like surface is emerged. In addition, it is illustrated that although TL is as anti-solvent, the thickness of perovskite film is approximately 240 nm and is slightly reduced with an increase in amount of TL dropping volume (from the SEM cross-sectional view that is shown in Fig. S2). Moreover, the roughness of films is slightly different and this may be attributed to the nucleation rate and inconsistent grain growth rate.

Table 1
Photovoltaic parameters of small-area perovskite solar cells obtained with different anti-solvents treatment.

	Voc (V)	Jsc (mA/cm^2)	FF	Efficiency (%)
w/o	0.27 ± 0.01	4.21 ± 0.21	0.30 ± 0.01	0.33 ± 0.02
TL	0.94 ± 0.05	19.93 ± 1.00	0.69 ± 0.03	12.85 ± 0.64
CF	0.88 ± 0.04	16.39 ± 0.82	0.63 ± 0.03	9.11 ± 0.46
CB	0.94 ± 0.05	19.22 ± 0.96	0.61 ± 0.03	10.88 ± 0.54
DCB	0.93 ± 0.05	19.01 ± 0.95	0.63 ± 0.03	11.12 ± 0.56
IPA	0.90 ± 0.04	12.32 ± 0.62	0.63 ± 0.03	7.00 ± 0.35

The standard deviation (s.d) is calculated from 8 cells.

Fig. 7**(a) and (b)** show the absorption spectra of the perovskite precursor treated with various TL dropping volumes before and after post-annealing. Before post-annealing, a very low absorption in the range of 400–850 nm is seen. This proves again that the perovskite precursor treated with different TL dropping volumes is transparent, and is an intermediate phase compound $MA_2Pb_3I_8(DMSO)_2$ [22]. After post-annealing, the intensity of the absorption spectra increases and the absorption edges are similar to a classical perovskite [26]. Furthermore, when the perovskite precursor is treated with 50 and 75 μl of TL, the absorption in the range of 400–850 nm is very similar. This indicates that both perovskite layers have good crystallinity. However, the perovskite precursor treated with 50 μl of TL shows a slightly lower absorption intensity in the range of 450–550 nm, which could affect the generation of the short-circuit current. The perovskite precursor treated with 25 μl of TL shows extremely low absorption intensity, which could be attributed to the light scattering effect by residual MAI or pinholes on the perovskite layer surface [35].

The top view of SEM images were used to evaluate the microstructure of the perovskite precursor treated with various TL dropping volumes and after post-annealing, as shown in Fig. 8**(a)** to **(d)**. The surface morphology clearly shows a discontinuous film with pinholes in the perovskite precursor treated with 25 μl of TL after post-annealing. When the TL dropping volume is increased to 50 μl, the pinholes disappear, and the perovskite grains become large. However, it is composed of many small grains within one domain. In addition, some deep valleys form on the perovskite layer surface, which could be the result of inconsistent nucleation rate and grain growth, affecting the coverage of the subsequent layer of PCBM. Once the TL dropping volume is increased to 75 μl, the topography as well the perovskite grains become more smooth and individual, indicating lower grain boundary density of the perovskite layer. In contrast, the perovskite grains become

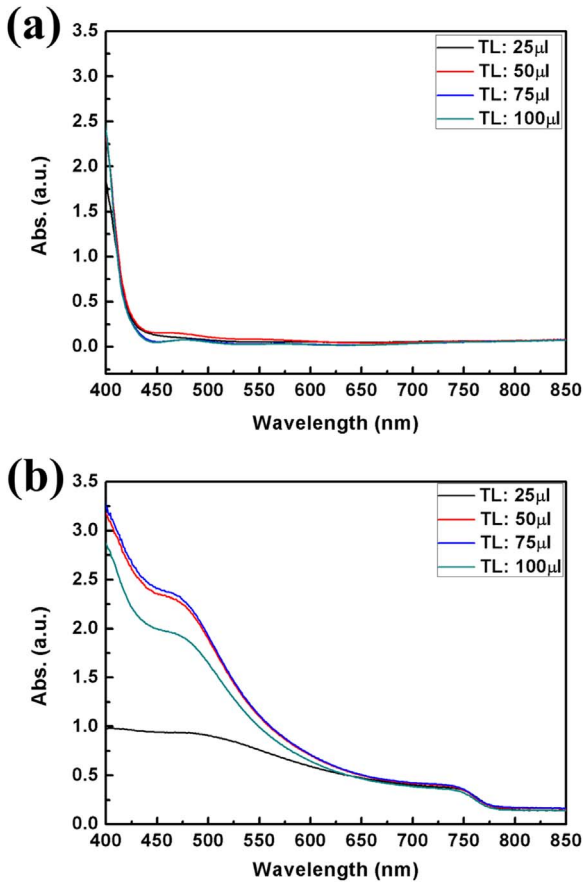

Fig. 7. The absorption spectra recorded from the perovskite precursor treated with different TL dropping volume (a) before and (b) after post-annealing.

obviously small and random when the TL dropping volume is increased to 100 μl. This may be caused by the removal of a large amount of the perovskite precursor, which results in the movement of the solution going closer to the supersaturation zone, causing the formation of several nucleation sites.

Table 2
Photovoltaic parameters of small-area perovskite solar cells obtained after treatment with different TL dropping volumes.

Volume	Voc (V)	Jsc (mA/cm^2)	FF	Efficiency (%)
25 μl	0.56 ± 0.03	10.76 ± 0.54	0.43 ± 0.22	2.59 ± 0.13
50 μl	0.89 ± 0.04	19.07 ± 0.95	0.67 ± 0.03	11.37 ± 0.57
75 μl	0.90 ± 0.05	21.76 ± 1.09	0.67 ± 0.03	13.12 ± 0.66
100 μl	0.83 ± 0.04	21.2 ± 1.06	0.61 ± 0.03	10.73 ± 0.54

The standard deviation (s.d) is calculated from 8 cells.

The photovoltaic characteristics of typical small-area perovskite solar cells treated with various TL dropping volumes under irradiation at 100 mW/cm^2 (AM 1.5 G), are shown in Fig. S3, and the photovoltaic characteristics of perovskite solar cells are summarized in Table 2. It is evident that the perovskite precursor treated with 75 μl of TL has the highest power conversion efficiency of 13.12%. This may be attributed to a flat surface and large individual perovskite grains (lower grain boundary density). In contrast, the perovskite precursor treated with 25 μl of TL shows a low power conversion efficiency of 2.57%. This is attributed to the pinholes and the discontinuous perovskite layer. The perovskite precursor treated with 50 μl TL displays the second highest PCE of 11.35%. It is slightly lower than the perovskite layer treated with 75 μl of TL since it is composed of many small grains in one domain. Similarly, the small perovskite grains in the case of the perovskite precursor treated with 100 μl of TL resulting in a PCE of 10.75%, which is lower than those treated with 50 and 75 μl. Moreover, the investigations on the volume of TL anti-solvent in the n-i-p type perovskite solar cell reveal the same results, which are shown in Fig. S4 and Table S2. According to the above results, it can be concluded the optimal volume ratio of the perovskite precursor to TL anti-solvent is 1:3 (v: v).

3.3. Preparation sub-model perovskite solar cell

The optimal anti-solvent and dropping volume had been well

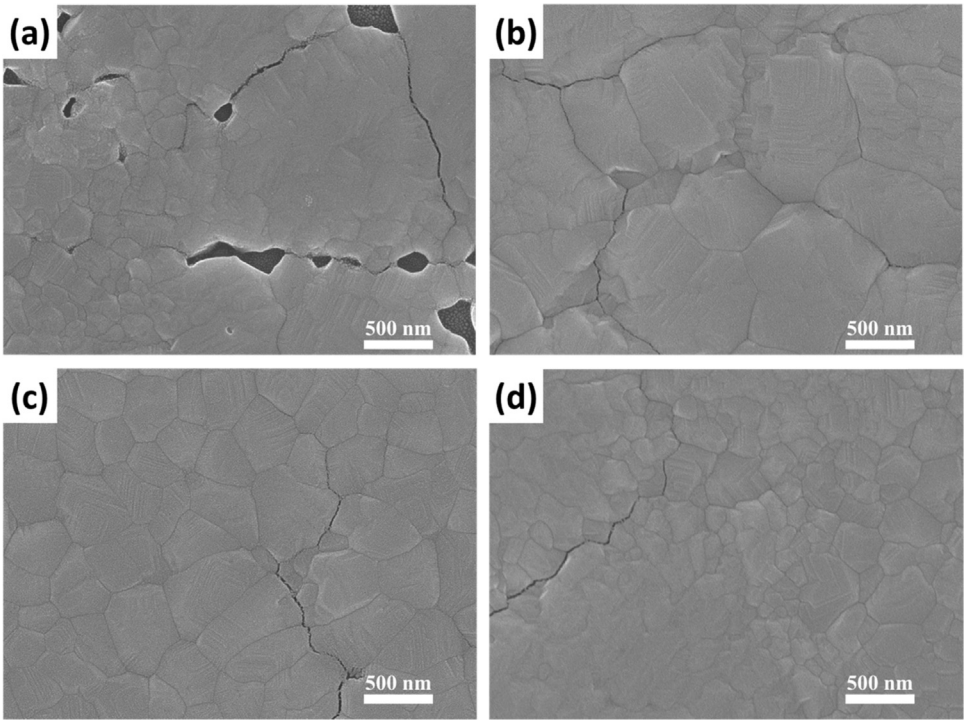

Fig. 8. The top-vise SEM images taken from the perovskite precursor, treated with (a) 25μl; (b) 50μl; (c) 75μl; (d) 100 μl, and suffers for post-annealing at 100 °C for 10 min.

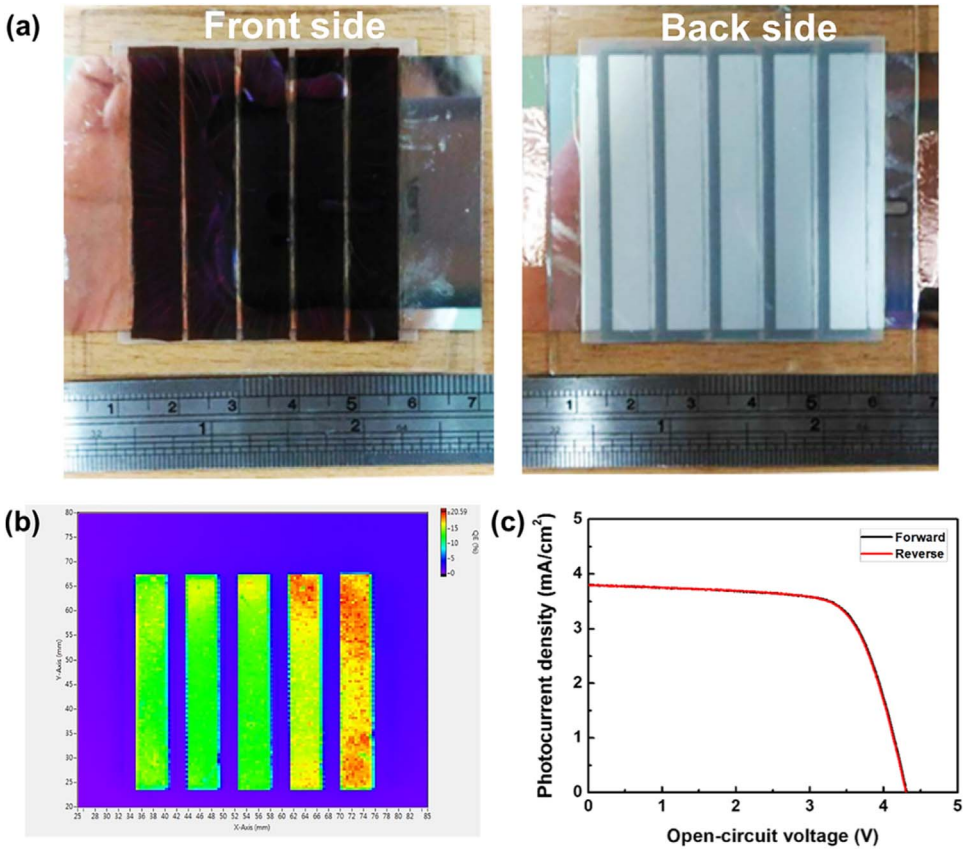

Fig. 9. (a) The photograph of sub-module perovskite solar cells (active area: 11.25 cm^2); **(b)** LBIC mapping of the 5 cm × 5 cm sub-module perovskite solar cell; (c) The J–V characteristics of the sub-module perovskite solar cell fabricated by TL anti-solvent drop casting.

investigated in the above section. In this section, we used TL as an anti-solvent, keeping the volume ratio of the perovskite precursor to anti-solvent as 1:3, where the solution volume was increased to 10 times (250μl:750μl) in preparing a larger area perovskite film. This demonstrates a sub-module perovskite solar cell that constructed from a series connection of five 2.25 cm^2 cells (substrate area: 25 cm^2 and active area: 11.25 cm^2). The photograph of the sub-module perovskite solar cell is shown in Fig. 9**(a)**. The CO_2-laser patterning process was adopted to fabricate an effective and integrated series connection between the cells in the module. The uniformity of the sub-module was revealed by Light Beam Induced Current (LBIC) mapping using an excitation wavelength of 532 (± 2 nm), as shown in Fig. 9**(b)**. The pattern in LBIC shows an unsymmetrical shape, rather than a symmetrical shape. This is due to the fact that single tube injection drop casting process with large amount of TL anti-solvent on large area substrate could cause the difference between the five single cells of the module, where the dropping of the anti-solvent fixed at a center position of film resulted in the different thickness in a circular distribution on the substrate (thinner at center and thicker at out ring) and the inhomogeneity of perovskite film.

From the sub-module perovskite solar cell, the J_{SC}, V_{OC}, fill factor (FF) and PCE of 3.79 mA/cm^2, 4.31 V, 0.71% and 11.60%, respectively, were achieved with negligible J-V hysteresis phenomena as seen in Fig. 9**(c)**, and its detailed photovoltaic characteristics are summarized in Table 3. A high PCE sub-module perovskite solar cell can be obtained through carefully selecting the anti-solvent as well as optimizing the volume ratio of the perovskite precursor to the anti-solvent. In this study, a further careful optimization of the perovskite film and PCBM layer deposition procedures could lead to a high PCE of perovskite solar module.

Table 3
Photovoltaic parameters of sub-module perovskite solar cells obtained after TL dropping treatment.

Scan direction	V_{OC} (V)	J_{SC} (mA/cm^2)	FF	Efficiency (%)
Forward scan	4.31	3.79	0.71	11.60
Reverse scan	4.30	3.80	0.71	11.60

4. Conclusions

In this study, it is concluded that: (a) the surface morphology and coverage of the perovskite layer can be significantly improved when introducing an anti-solvent with a low dielectric constant and low dipole moment into the drop casting process. This is attributed to the fact that the anti-solvent will drive the perovskite precursor into the metastable zone instead of the supersaturation zone. This increases the nucleation rate and grain growth rate consistent during the post-annealing process; (b) the optimal volume ratio of the perovskite precursor and the TL anti-solvent is 1:3. Using this volume ratio, the small-area and sub-module perovskite solar cells with PCE of 13.12% and 11.60%, respectively, were successfully achieved with negligible J-V hysteresis.

Acknowledgements

The authors acknowledge the financial support of the Ministry of Science and Technology, Taiwan (Grant number: MOST 104–2731-M-182-001-MY2 and MOST 106–2218-E-182 -005 -MY2) and the financial support of Chang Gung Memorial Hospital, Linkou, Taiwan (CMRPD2F0161 and BMRPC074).

Appendix A. Supporting information

Supplementary data associated with this article can be found in the online version at http://dx.doi.org/10.1016/j.solmat.2017.08.010.

References

[1] A. Kojima, K. Teshima, Y. Shirai, T. Miyasaka, J. Am. Chem. Soc. 131 (2009) 6050–6051.
[2] NRRL chart, ⟨http://www.nrel.gov/ncpv/images/efficiency_chart.jpg⟩, (Accessed 13 March 2016).
[3] M.A. Green, A. Ho-Baillie, H.J. Snaith, Nat. Photon 8 (2014) 506–514.
[4] A. Miyata, A. Mitioglu, P. Plochocka, O. Portugall, J.T.-W. Wang, S.D. Stranks, H.J. Snaith, R.J. Nicholas, Nat. Phys. 11 (2015) 582–587.
[5] S.D. Stranks, G.E. Eperon, G. Grancini, C. Menelaou, M.J.P. Alcocer, T. Leijtens, L.M. Herz, A. Petrozza, H.J. Snaith, Science 342 (2013) 341–344.
[6] G.E. Eperon, S.D. Stranks, C. Menelaou, M.B. Johnston, L.M. Herz, H.J. Snaith, Energy Environ. Sci. 7 (2014) 982–988.
[7] S.D. Stranks, H.J. Snaith, Nat. Nano 10 (2015) 391–402.
[8] M.M. Lee, J. Teuscher, T. Miyasaka, T.N. Murakami, H.J. Snaith, Science 338 (2012) 643–647.
[9] L. Hu, J. Peng, W. Wang, Z. Xia, J. Yuan, J. Lu, X. Huang, W. Ma, H. Song, W. Chen, Y.-B. Cheng, J. Tang, ACS Photonics 1 (2014) (547-533).
[10] M. Liu, M.B. Johnston, H.J. Snaith, Nature 501 (2013) 395–398.
[11] L. Hu, J. Peng, W. Wang, Z. Xia, J. Yuan, J. Lu, X. Huang, W. Ma, H. Song, W. Chen, Y.-B. Cheng, J. Tang, ACS Photonics 1 (2014) 547–553.
[12] L. Meng, J. You, T.-F. Guo, Y. Yang, Acc. Chem. Res. 49 (2015) 155–165.
[13] Y. Shao, Z. Xiao, C. Bi, Y. Yuan, J. Huang, Nat. Commun. 5 (2014).
[14] Y. Shao, Y. Yuan, J. Huang, Nat. Energy 1 (2016) 15001.
[15] C. Bi, Q. Wang, Y. Shao, Y. Yuan, Z. Xiao, J. Huang, Nat. Commun. 6 (2015).
[16] T. Salim, S. Sun, Y. Abe, A. Krishna, A.C. Grimsdale, Y.M. Lam, J. Mater. Chem. A 3 (2015) 8943–8969.
[17] M.A. Green, K. Emery, Y. Hishikawa, W. Warta, E.D. Dunlop, Prog. Photovolt.: Res. Appl. 23 (2015) 805–812.
[18] Y. Wu, X. Yang, W. Chen, Y. Yue, M. Cai, F. Xie, E. Bi, A. Islam, L. Han, Nat. Energy 1 (2016) 16148.
[19] W. Yongzhen, A. Islam, X. Yang, C. Qin, J. Liu, K. Zhang, W. Peng, L. Han, Energy Environ. Sci. 7 (2014) 2934–2938.
[20] Q. Chen, H. Zhou, Y. Fang, A.Z. Stieg, T.-B. Song, H.-H. Wang, X. Xu, Y. Liu, S. Lu, J. You, P. Sun, J. McKay, M.S. Goorsky, Y. Yang, Nat. Commun. 6 (2015).
[21] N.J. Jeon, J.H. Noh, Y.C. Kim, W.S. Yang, S. Ryu, S.I. Seok, Nat. Mater. 13 (2014) 897–903.
[22] Y. Rong, S. Venkatesan, R. Guo, Y. Wang, J. Bao, W. Li, Z. Fan, Y. Yao, Nanoscale 8 (2016) 12892–12899.
[23] B. Xia, Z. Wu, H. Dong, J. Xi, W. Wu, T. Lei, K. Xi, F. Yuan, B. Jiao, L. Xiao, Q. Gong, X. Hou, J. Mater. Chem. A 4 (2016) 6295–6303.
[24] Y. Zhou, M. Yang, O.S. Game, W. Wu, J. Kwun, M.A. Strauss, Y. Yan, J. Huang, K. Zhu, N.P. Padture, ACS Appl. Mater. Interfaces 8 (2016) 2232–2237.
[25] X. Zheng, B. Chen, C. Wu, S. Priya, Nano Energy 17 (2015) 269–278.
[26] Y. Zhou, M. Yang, A.L. Vasiliev, H.F. Garces, Y. Zhao, D. Wang, S. Pang, K. Zhu, N.P. Padture, J. Mater. Chem. A 3 (2015) 9249–9256.
[27] F. Hao, C.C. Stoumpos, P. Guo, N. Zhou, T.J. Marks, R.P.H. Chang, M.G. Kanatzidis, J. Am. Chem. Soc. 137 (2015) 11445–11452.
[28] Y.-C. Chern, H.-R. Wu, Y.-C. Chen, H.-W. Zan, H.-F. Meng, S.-F. Horng, AIP Adv. 5 (2015) 087125.
[29] W. Nie, H. Tsai, R. Asadpour, J.-C. Blancon, A.J. Neukirch, G. Gupta, J.J. Crochet, M. Chhowalla, S. Tretiak, M.A. Alam, H.-L. Wang, A.D. Mohite, Science 347 (2015) 522–525.
[30] Y. Zhou, M. Yang, W. Wu, A.L. Vasiliev, K. Zhu, N.P. Padture, J. Mater. Chem. A 3 (2015) 8178–8184.
[31] J. Liu, C. Gao, X. He, Q. Ye, L. Ouyang, D. Zhuang, C. Liao, J. Mei, W. Lau, ACS Appl. Mater. Interfaces 7 (2015) 24008–24015.
[32] H. Chen, Z. Wei, H. He, X. Zheng, K.S. Wong, S. Yang, Adv. Energy Mater. 6 (2016) (n/a-n/a).
[33] S. Pang, Y. Zhou, Z. Wang, M. Yang, A.R. Krause, Z. Zhou, K. Zhu, N.P. Padture, G. Cui, J. Am. Chem. Soc. 138 (2016) 750–753.
[34] C.-H. Chiang, Z.-L. Tseng, C.-G. Wu, J. Mater. Chem. A 2 (2014) 15897–15903.
[35] D.-Y. Son, J.-W. Lee, Y.J. Choi, I.-H. Jang, S. Lee, P.J. Yoo, H. Shin, N. Ahn, M. Choi, D. Kim, N.-G. Park, Nat. Energy 1 (2016) 16081.
[36] S.A. Kulkarni, A.S. Myerson, Reversible control of solubility using functionalized nanoparticles, Chem. Commun. 53 (2017) 1429–1432.